Journal of Research and Applications in Mechanical Engineering
ISSN: 2229-2152 (Print); 2697-424x (Online)
(2022) Vol. 10, No. 2, Paper No. JRAME-22-10-008
DOI: 10.14456/jrame.2022.8

Research Article

VISUALIZATION OF SOOT NANOSTRUCTURE FROM ETHANOL BLENDED BIODIESEL USING ELECTRON MICROSCOPY IMAGE ANALYSES

Myat Hsu Thin[1]
P. Karin[1]
M. Srilomsak[1],*
W. Po-ngen[2]
P. Saisirirat[3]
N. Chollacoop[3]
H. Kosaka[4]
[1] *School of Engineering, King Mongkut's Institute of Technology Ladkrabang, Bangkok 10520, Thailand*
[2] *Faculty of Technical Education, King Mongkut's University of Technology North Bangkok, Bangkok 10800, Thailand*
[3] *National Energy Technology Center, National Science and Technology Development Agency, Pathum Thani 12120, Thailand*
[4] *School of Engineering, Tokyo Institute of Technology, Tokyo 152-8552, Japan*

Received 21 June 2022
Revised 16 July 2022
Accepted 20 July 2022

ABSTRACT:
Characteristics of particulate matter from ethanol-blended biodiesel on the diesel engine in terms of nanostructure were investigated through electron microscopy. Commercial B20 fuel (20% palm and 80% diesel) was used as the baseline fuel and ethanol was blended at 5% and 10% with B20 fuel. The agglomerated particle size was reduced by increasing the weight ratio of ethanol. The average diameter sizes of the single primary nanoparticles of B20, B20E5, and B20E10 are about 20-40 nm while inter-planar spacing is about 0.404 nm, 0.383 nm, and 0.352 nm, respectively. The total fringe lengths of B20, B20E5, and B20E10 are approximately 521 nm, 470 nm, and 262 nm measured from the areas of 20 nm x 20 nm of primary nanoparticles.

Keywords: *Particulate Matter, Electron Microscopy, Diesel Engine, Biodiesel, Soot nanostructure*

1. INTRODUCTION

Air pollution is caused by a variety of sources. One of the most significant sources of air pollution in cities is vehicle emissions [1]. Electric vehicles are gaining popularity around the world as a major means of reducing greenhouse gas and other harmful pollutants [2, 3]. However, compression ignition, or diesel, engines will continue to be the primary source of power for heavy-duty trucks, and demand will remain strong [4]. This is due to the fact that the diesel engine is one of the most fuel-efficient and thermally efficient internal combustion engines available. But, different types of emissions, including particulate matter emissions, are generated into the surrounding air because of fossil fuel combustion in internal combustion engines, posing a major threat to both the environment and human health [5].

Particulate matter (PM) is released from an internal combustion engine during fuel-rich operating conditions, which means there is not enough oxygen in the combustion chamber for complete combustion [6]. PM 2.5 and PM10 are major risks of human health effects in the breathing of airborne particles and urban air pollution issues [7]. There are

* Corresponding author: M. Srilomsak
E-mail address: mek.sr@kmitl.ac.th

two major solutions to reduce PM from diesel engine exhaust: reducing during the formation process of PM or reducing PM after the production process with devices. PM can be reduced in the formation process by using fuel additives or, in this research, using ethanol-blended biodiesel at 5% and 10% with the baseline B20 biodiesel.

Many studies have shown that biodiesel blended diesel fuels are compatible with all diesel engines and that particle emissions can be greatly decreased [8]. Biodiesel made from palm oil is widely utilized in Thailand, where it is combined with diesel fuel as B7 (7 percent biodiesel), B10 (10 percent biodiesel), and B20 (20 percent biodiesel). Unlike biodiesel, ethanol has large volumes of feedstock because it can be made in Thailand from sugarcane juice, cassava, and molasses. However, due to the poor miscibility of ethanol in diesel fuel, there is a significant barrier to using ethanol – diesel blended fuels. This phase separation is affected by the temperature, the chemical composition of the diesel fuel, and the proportion of ethanol introduced [9, 10]. M. Hanna demonstrated that adding biodiesel to the fuel stream improves E-diesel miscibility by acting as an amphiphile (a surface-active agent) and producing micelles with polar heads and nonpolar tails [11]. The nonpolar tail of the biodiesel molecule was oriented with the diesel molecule, while the polar head was adapted with the ethanol molecule. This feature of biodiesel can keep micelles in a thermodynamically stable condition, allowing for higher ethanol percentages in blends.

Furthermore, methyl ester biodiesel is more soluble than ethyl and butyl ester biodiesel [12]. M. Tongroon's study group investigated the stability of ethanol in diesel-biodiesel-ethanol blends in various ethanol percent at room temperature (27-30 °C) and Thailand's lowest winter temperature (5 °C) [13]. At both temperatures, the results demonstrated that Thailand's commercial B20 fuel can blend up to 20% ethanol without phase separation in three months. Different co-solvents and emulsifiers have been used to study diesel-ethanol bends in various diesel engines. Many studies have demonstrated that diesohol gasoline can reduce particulate matter (PM) emissions while also increasing fuel consumption. Kass et al [14] looked at the impact of E-diesel on emissions from a heavy-duty engine. They mixed 10% and 15% ethanol with diesel fuel and found that both mixes resulted in an 8 percent reduction in engine output torque. The results showed that ethanol may greatly reduce PM and smoke emissions, although carbon monoxide (CO) and nitrogen oxides (NOx) emissions were dependent on the test conditions. However, analysis in terms of particulate matter morphology and nanostructure has not been fully investigated.

This research aims to investigate the effect of ethanol on the PM in terms of morphology and nanostructure and compare by using electron microscopy. Morphology of agglomerate structure, primary particle size, fringe length distribution, and inter-planer of soot were analyzed.

2. MATERIALS AND METHODS

2.1 Particulate matter collection

The experiment was conducted on the 3L 4-cylinder common rail direct diesel injection engine at different engine operations. The engine specifications are shown in Table 1. This research was conducted using three fuels: (1) commercial biodiesel (B20, 20% biodiesel, and 80% diesel) was used as a baseline fuel, (2) B20E5 (blended sample of 5%wt ethanol with 95%wt B20) and B20E10 (blended sample of 10%wt ethanol with 90%wt B20). The standards by which the fuel properties from Table 2 are also included. After testing under numerous engine speeds and loads for each fuel, the soot powder was collected from the exhaust pipe. Paper filters were used with a BOSCH smoke meter (Okuda DSM – 240) to collect soot for examining the agglomerate particles. The accuracy of the sensors and measurement devices is also described in Table 3.

2.2 TEM and SEM Particle Analysis

SEM (FE-SEM SU8200) under 10,000 magnification was used to investigate the paper filters holding engine-born agglomeration particles. The size of the agglomeration particles was then calculated using ImageJ, an image processing software. To investigate the morphology and size of the soot particles, the PM powders were analyzed with a TEM (JEM-2100Plus) at magnifications of 30,000 and 80,000. The size of the single primary particles was figured out by analyzing the 30,000 magnification images for the PM with ImageJ. To investigate the nanostructure and graphite crystallite of the particles, the 80,000 magnification images for the PM were converted to black and white, then skeletonized using ImageJ.

Table 1: Engine Specifications.

Parameters	Value
Model	ISUZU 4JJ1 TC
Engine Type	Diesel, four strokes
No of cylinders	Inline-four cylinders
Bore	95.4 mm
Stroke	104.9 mm
Total Displacement	3000 cc
Compression ratio	18.3:1
Injection System	Common Rail
Maximum power output	107 kW@3600 rpm
Maximum torque output	294 Nm @ 1400-3400 rpm

Table 2: Fuel Properties

Fuel Properties	Standard	B20	Ethanol	B20E5	B20E10
Carbon (% mass)	ASTM D 5291	82.61	52.2	-	-
Hydrogen (% mass)	ASTM D 5291	13.45	13	-	-
Oxygen (% mass)	ASTM D 5291	13.94	34.8	-	-
Calorific Value (MJ/kg)	ASTM D 240	44.95	28.05	43.95	42.72
Viscosity @ 40°C (mm^2/s)	ASTM D 445	3.1	1.2	2.69	2.49
Density @ 25°C (kg/m^3)	ASTM D 1298	827	789	824	822
T10		177.4	77.8		
T90		348.4	80		

Table 3: Accuracy of Sensors and Measurement Devices

Devices	Accuracy
Eddy current dynamometer (rpm)	± 5
Eddy current dynamometer (load %)	± 0.8%
Weight scale (g)	± 0.15
Pressure sensor (bar)	± 0.5
CA encoder (deg)	± 0.2
Thermocouple (°C)	± 2.2
Bosch smoke meter (%)	± 3%

3. RESULT AND DISCUSSION

In this research, the morphology, and nanostructure of the PM from the baseline B20 fuel and ethanol-blended fuels were investigated by using electron microscopy because we would like to find the soot that can be easily trapped and oxidized. Soot size and nanostructure are related to the oxidation rates and smaller agglomerate particles show higher filtration efficiency when the after-treatment system is applied at the outlet of the exhaust [15]. Therefore, the structure of soot particles was studied as a first step, and then this will be compared with the soot oxidation rates in a future study.

3.1 Soot Morphology

Based on 10k magnification scanning electron microscopy (SEM) images of paper filters, the distribution of agglomerated particle size and the average agglomeration size were analyzed (Fig. 1.) ImageJ tool had been used to measure a hundred agglomeration particles. The particle size distributions are shown in Fig. 2(a), and there is a tendency in which the agglomerate distribution curve shifts to the left, or the size reduces, as the ethanol content rises. The mean agglomerate particle sizes of B20, B20E5, and B20E10 are 1.01 µm, 0.52 µm, and 0.42 µm, respectively (see Fig. 2b). According to the results, soot agglomerate sizes from ethanol-blended fuels are smaller than those from B20 fuels as the ethanol-blended biodiesel has less carbon content compared to oxygen content which will be used for the soot oxidation.

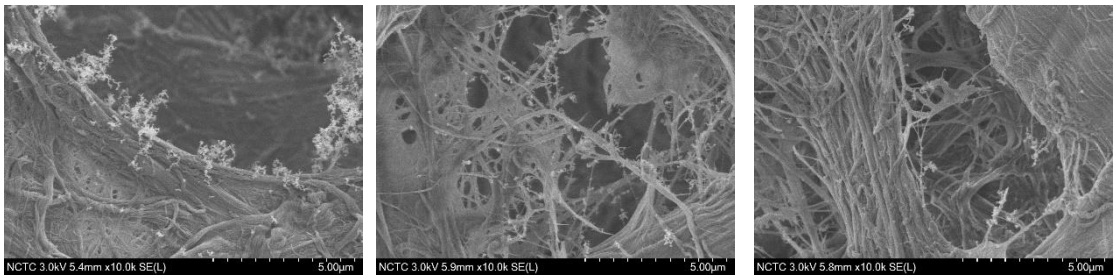

(a) (b) (c)

Fig. 1. 10k Magnification Scanning Electron Microscopy (SEM) images of (a) B20, (b) B20E5 and (c) B20E10

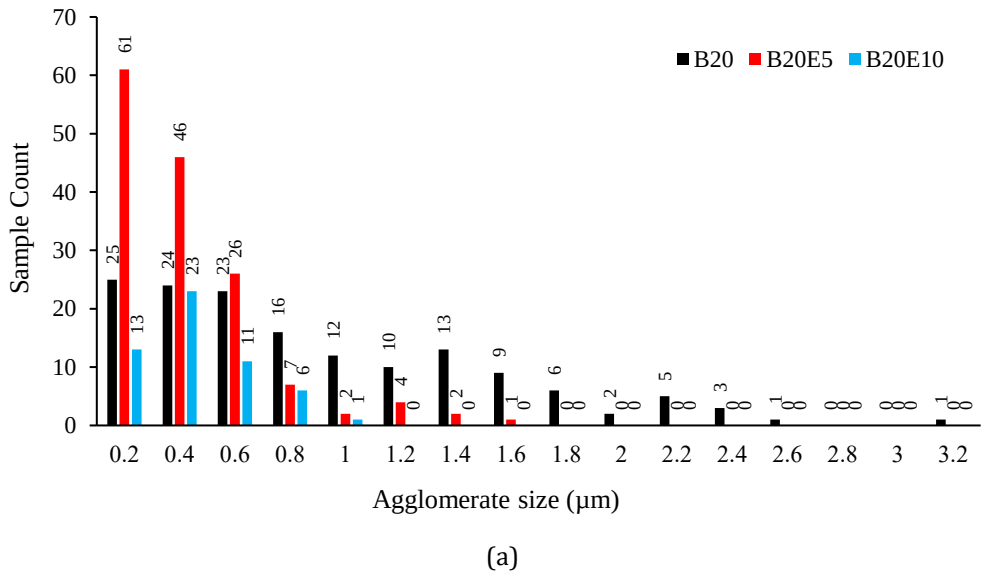

(a)

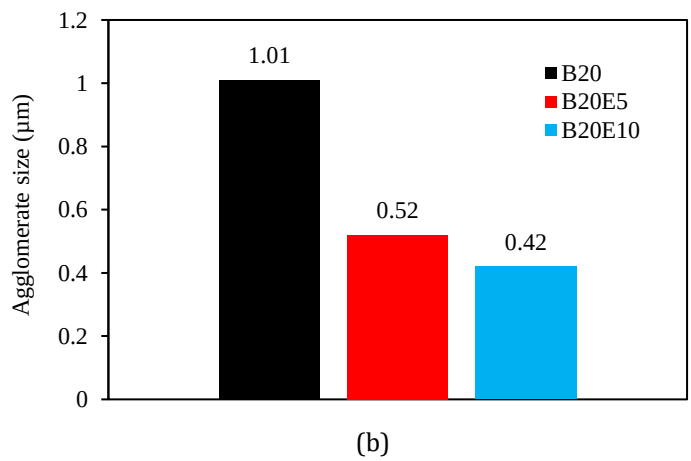

(b)

Fig. 2. (a) Agglomerate Particle Size Distribution and (b) Average Agglomerate Particle Size of B20, B20E5, and B20E10

The morphology of single particles was studied using the x30,000 magnification TEM. Single primary particles have aggregated with similar morphologies to form an agglomeration structure of nanoparticles that is mostly made up of spherical primary particles. According to the TEM images, the morphology of the agglomerate structure of soot from ethanol-blended biodiesel is distinguishable from the baseline B20 fuel, as shown in Fig. 3(a-c). The nanostructure of single primary particles was also investigated using TEM, and high-quality images were produced. Fig.4 (a-c)

shows the nanostructure of soot at a magnification of x800,000. Single primary particles have a spherical nanostructure made up of curve line carbon crystallites.

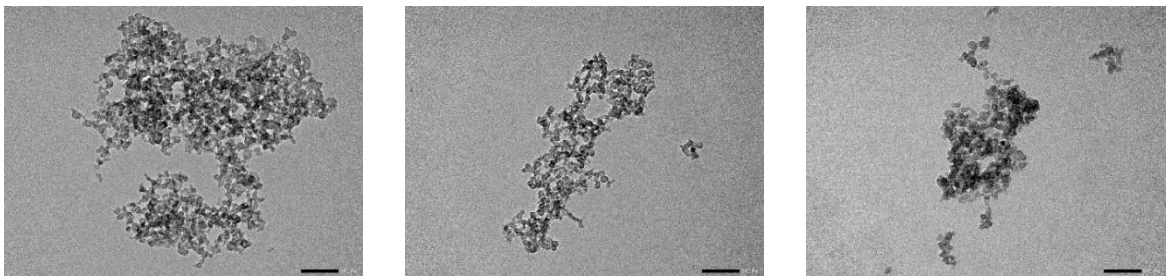

(a) (b) (c)

Fig. 3. TEM images of the agglomerate structure of fine particles of PMs from (a) B20, (b) B20E5, and (c) B20E10

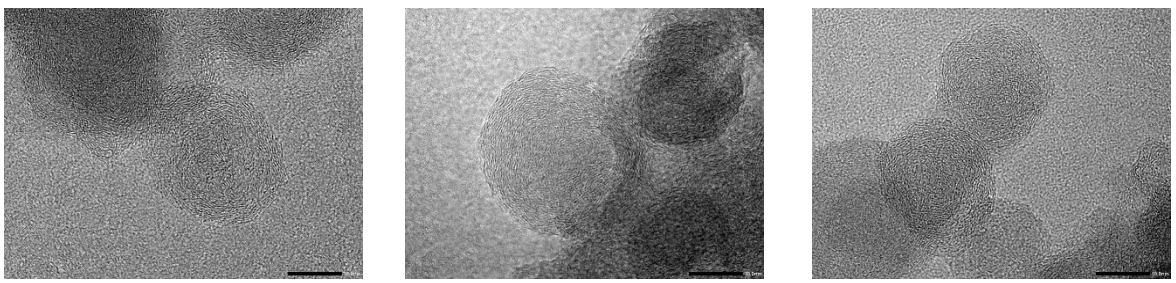

(a) (b) (c)

Fig. 4. TEM images of Single Primary Particles of Soot with high magnifications (x800k) from (a) B20 (b) B20E5, and (c) B20E10

Furthermore, the single primary particle sizes were successfully measured using the TEM image processing method by ImageJ software. This software randomly measured about one hundred single primary particles from various samples to determine primary particle size. The size distribution of single primary nanoparticle observations, which ranged from 10 nm to 65 nm, is represented in Fig. 5. The peaks of the soot histogram were detected in particle sizes of 20 nm and 25 nm in the particle distribution. The average diameter of soot nanoparticles from B20, B20E5, and B20E10 was 33 nm, 28 nm, and 25 nm, respectively. Therefore, the primary particle diameter of soot becomes smaller with increasing the ethanol percentage, this result is consistent with another study by Jeff Ho et al. in 2016. The study reported that increased ethanol content results in a reduction of the nuclei particle by lowering the carbon content and raising the oxygen level [16].

3.2 Fringe length analysis of soot

The fringe length study was conducted using a 20 nm x 20 nm squared section of single primary particles nanostructure to evaluate the differences in soot crystalline structure using a TEM image processing method. To construct the skeletonized nanostructure, the regions in TEM images were first specified in single primary particles, then cropped into the specified region. They were then transformed into binary black and white graphics. Finally, skeletonized images were generated from TEM images. Figures 6, 7, and 8 show how image processing was used to analyze skeletonized pictures of soot to determine the fringe length and inter-planar spacing in the case of B20, B20E5 and B20E10, respectively. Both the baseline fuel and the ethanol-blended fuel are qualitatively similar as they are predominantly made up of curved lines of carbon crystallites, according to the skeletonized nanostructures study.

TEM image processing methods had been used to quantitatively analyze all the fringes from each of the skeletonized photos of single primary particles for the fringe length distribution. Figure 9 shows the fringe length distribution from the required areas that were cropped in 20 nm × 20 nm. The fringe length distribution revealed that all carbon crystallite fringe lengths are primarily in the range of 0.2 nm to 6 nm. The majority of fringes in the fringe length distribution were between 0.2 and 1 nm, with the highest peaks in the 0.5 and 1 nm range. The average fringe lengths of B20, B20E5, and B20E10 were 1.28, 1.17, and 0.72 nm, respectively: with decreasing the fringe length as the

ethanol percentage increased. According to Zygogianni et al., higher reaction rates are achieved with shorter fringes, but the mass fraction at the maximum activation energy decreases [17]. The observed tendency generally indicates that the shorter the fringe length, the more reactive carbon material. It could be pointed out that fringe length is an accurate measure of the structural order and reactivity of carbonaceous materials [18].

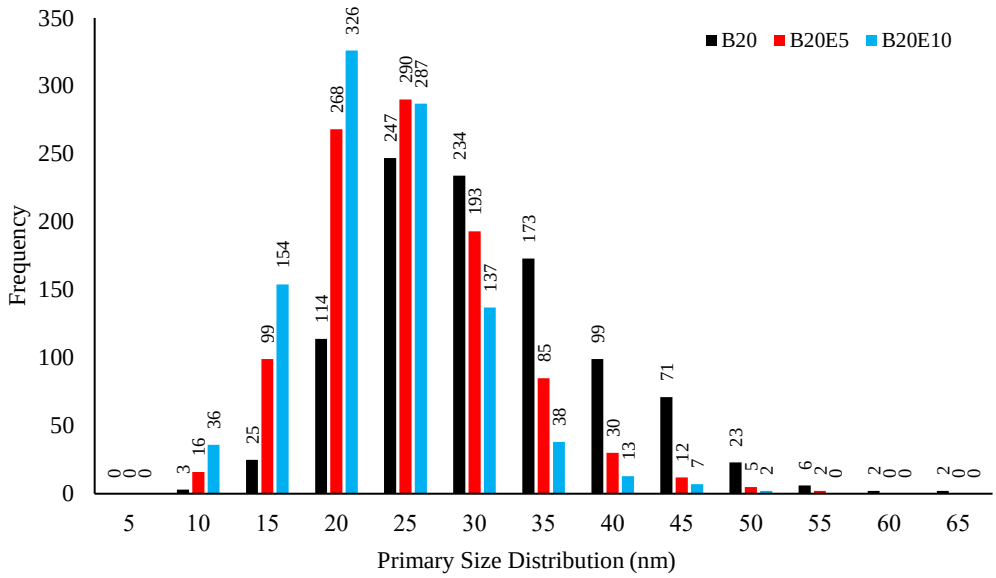

Fig. 5. Single Primary Size Distribution of PMs from B20, B20E5, and B20E10

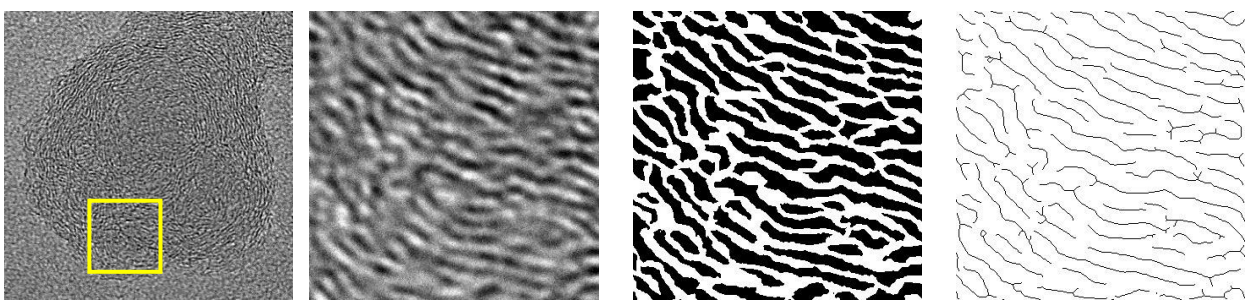

Fig. 6. TEM Images of Nanostructure of B20 (a) specified area (b) (20nm x 20nm) cropped image (c) black and white binary image, and (d) skeletonized images of soot crystal

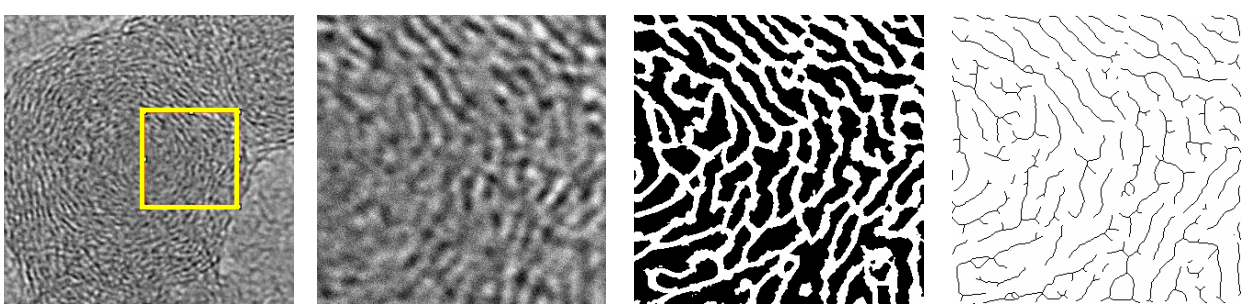

Fig. 7. TEM Images of Nanostructure of B20E5 (a) specified area (b) (20nm x 20nm) cropped image (c) black and white binary image, and (d) skeletonized images of soot crystal

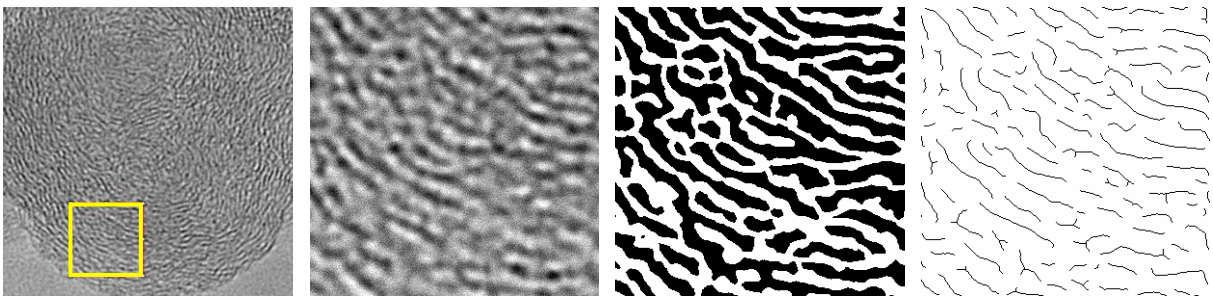

Fig. 8. TEM Images of Nanostructure of B20E10 (a) specified area (b) (20nm x 20nm) cropped image (c) black and white binary image, and (d) skeletonized images of soot crystal

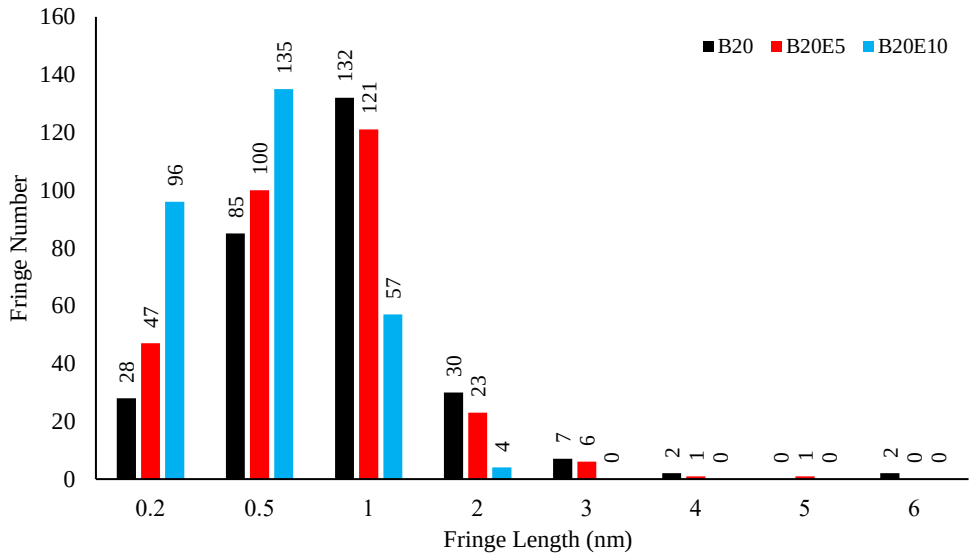

Fig. 9. Fringe Length Distribution of Single Primary Nanoparticles from B20, B20E5, and B20E10

Moreover, the space between the carbon crystallites was well-defined as the inter-planar spacing of soot. The values of inter-planar spacing were approximately 0.404 nm, 0.383 nm, and 0.352 nm of B20, B20E5, and B20E10. The quantitative study of various soot nanoparticles was shown using fringe analyses with fringe length and inter-planar spacing. The analyses provided useful information for determining the density of soot.

4. CONCLUSION

The soot from different ethanol contents with biodiesel and baseline B20 fuel was collected and studied. In terms of size distribution, SEM and TEM were used to examine the morphology of soot agglomerate particles and single primary particles. The ethanol content and distribution curve have a relationship, as seen by these distributions. As the ethanol concentration increased, the distribution curve shifted left, implying that the size of both agglomeration particles and single primary particles decreased. A relationship between ethanol content and carbon crystalline structure fringe can also be seen in the fringe length and inter-planar spacing analyses. As the ethanol percentage increased, the average and largest fringe lengths decreased. The spacing and ethanol content relationship are likewise similar to the size distribution and fringe length and ethanol percent relationship.

The crystalline and amorphous carbon structure will be further investigated using X-ray diffraction (XRD) and Raman Spectroscopy (RS) and then compared with other literature. The oxidation of the particulate matter will also be investigated in future research using Thermogravimetric analysis (TGA).

ACKNOWLEDGMENTS

The authors would like to thank the National Research Council of Thailand (Diesel Engine's Particulate Matter Reduction using Ethanol-Biodiesel-Diesel Blends and Particulate Filter 398/2563) and King Mongkut's Institute of Technology Ladkrabang for their support.

REFERENCES

[1] Vichit-Vadakan, N. and Vajanapoom, N. Health impact from air pollution in Thailand: Current and future challenges, Environmental Health Perspectives, Vol. 119(5), 2011, pp. A197-A198.
[2] Choi, H. Technology-push and demand-pull factors in emerging sectors: evidence from the electric vehicle market, Industry and Innovation, Vol. 25(7), 2018, pp. 655-674.
[3] Hertzke, P., Müller, N. and Schenk, S. Dynamics in the global electric-vehicle market, McKinsey Center for Future Mobility, 2017.
[4] Askin, A., Barter, G., West, T. and Manley, D. The heavy-duty vehicle future in the United States: A parametric analysis of technology and policy tradeoffs, Energy Policy, Vol. 81, 2015, pp. 1-13.
[5] Maricq, M.M. Chemical characterization of particulate emissions from diesel engines: A review, Journal of Aerosol Science, Vol. 38(11), 2007, pp. 1079-1118.
[6] Heywood, J.B. Internal Combustion Engine Fundamentals, 1998, McGraw Hill, New York.
[7] Cheng, X., Huang, Y., Zhang, S.P., Ni, S.J. and Long, Z.J. Characteristics, sources, and health risk assessment of trace elements in PM10 at an urban site in Chengdu, Southwest China, Aerosol and Air Quality Research, Vol. 18(2), 2018, pp. 357-370.
[8] Tripatara, A., Karin, P., Phairote, W., Charoenphonphanich, C., Masomtob, M., Chollacoop, N., et al. Effect of biodiesel on compression ignition engine's combustion behavior and particle emission, Journal of Research and Applications in Mechanical Engineering, Vol. 8(2), 2020, pp. 92-100.
[9] Sayin, C. Engine performance and exhaust gas emissions of methanol and ethanol-diesel blends, Fuel, Vol. 89(11), 2010, pp. 3410-3415.
[10] Rakopoulos, D.C., Rakopoulos, C.D., Papagiannakis, R.G., Kyritsis, D.C. Combustion heat release analysis of ethanol or n-butanol diesel fuel blends in heavy-duty DI diesel engine, Fuel, Vol. 90(5), 2011, pp. 1855-1867.
[11] Fernando, S. and Hanna, M. Development of a novel biofuel blend using ethanol-biodiesel-diesel microemulsions: EB-diesel, Energy & Fuels, Vol. 18(6), 2004, pp. 1695-1703.
[12] Chotwichien, A., Luengnaruemitchai, A. and Jai-In, S. Utilization of palm oil alkyl esters as an additive in ethanol-diesel and butanol-diesel blends, Fuel, Vol. 88(9), 2009, pp. 1618-1624.
[13] Tongroon, M., Saisirirat, P., Suebwong, A., Aunchaisri, J., Kananont, M. and Chollacoop, N. Combustion and emission characteristics investigation of diesel-ethanol-biodiesel blended fuels in a compression-ignition engine and benefit analysis, Fuel, Vol. 255, 2019, Article number: 115728.
[14] Kass, M.D., Thomas, J.F., Storey, J.M., Domingo, N., Wade, J. and Kenreck, G. Emissions from a 5.9 liter diesel engine fueled with ethanol diesel blends, SAE Technical Paper, 2001, Article number: 2001-01-2018.
[15] Lefort, I., Herreros, J. and Tsolakis, A. The use of a partial flow filter to assist the diesel particulate filter and reduce active regeneration events, SAE International Journal of Engines, Vol. 7(4), 2014, pp. 1953-1960.
[16] Tse, H., Leung, C.W. and Cheung, C.S. Performances, emissions and soot properties from a diesel-biodiesel-ethanol blend fuelled engine, Advances in Automobile Engineering, Vol. S1, 2016, pp. 1-7.
[17] Zygogianni, A., Syrigou, M., Konstandopoulos, A.G. and Kostoglou, M. Oxidative reactivity of particulate samples from different diesel combustion systems and its relation to structural and spectral characteristics of soot, Emission Control Science and Technology, Vol. 5, 2019, pp. 99-123.
[18] Vander Wal, R.L. and Mueller, C.J. Initial investigation of effects of fuel oxygenation on the nanostructure of soot from a direct-injection diesel engine, Energy Fuel, Vol. 20(6), 2006, pp. 2364-2369.